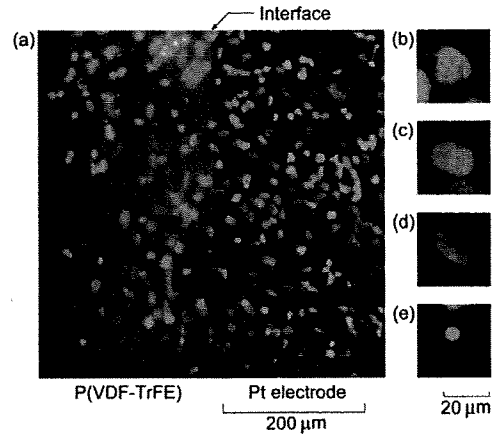

Fig. 4 (a) Fluorescent photograph of cultured neurons over P(VDF-TrFE) film and Pt electrode modified by fibronectin on Si substrate; (b)~(d) distorted stained area corresponding to living neurons and (e) circular area corresponding to dead one.

photograph. Although it is relatively difficult to strictly distinguish between the neuron and the glia cell only from Fig.4 (a), it is found that there are many stained areas with distorted shape. These distorted stained areas correspond to the living neurons or glia cells which adhere on the surface of substrate, where typical distorted and stained areas are shown in Fig.4 (b)~(d). In contrast, the dead cells should have a circular shape as shown in Fig.4 (e), because they do not adhere on the surface of materials. It is found that there are few dead cells in Fig. 4(a). In terms of cell viability, there is no qualitative difference between the area of the P(VDF-TrFE) and the Pt electrode. It may be because the surfaces are uniformly modified by the fibronectin. Furthermore, it is confirmed that there are living neurons or glia cells on the interface between P(VDF-TrFE) and the electrode. From these result, it can be concluded that the Pt thin film electrode is biocompatible and the electrodes must work well for stimulating neurons on it. Consequently, the biocompatibility of proposed artificial cochlea is also confirmed in cytotoxicity. In addition, it is important to discuss the *in vivo* biocompatibility in the context of sensitization, irritation, chronic toxicity, genotoxicity, and fibrous encapsulation.

The present study provides the fundamental knowledge on the biocompatibility of MEMS fabricated P(VDF-TrFE) films and proposed artificial cochlea. However, from the viewpoint of ABM's vibrating characteristics, the neurons should not be cultured on the flexible ABM as shown in Fig. 1(b), since the eigen frequency of vibration is designed before the implantation into a cochlea[7], where the effect of neurons on the vibration is not considered. On the contrary, the neurons should be cultured on the electrodes to be stimulated effectively. Thus, the area where neurons are cultured should be controlled by patterning the cell adhesion factor using MEMS technologies[16], where it is our future work.

4. Concluding remarks

In the present paper, the biocompatibility of fully self-contained implantable artificial cochlea which is made of P(VDF-TrFE) film, the Pt electrodes, and the Si substrate by MEMS and thin films technologies was studied by culturing cerebral cortical neurons from rats. The neurons were successfully cultured on the P(VDF-TrFE) film modified by the fibronectin and the collagen. From the phase contrast photographs, it was found that dendrites and an axon were extended from a soma of a neuron. No qualitative difference in terms of viability of neurons was found between the fibronectin and the collagen.

Furthermore, the neurons were successfully cultured over the P(VDF-TrFE) film and the Pt thin film electrode for the implantable artificial cochlea. Consequently, it was confirmed that the MEMS fabricated P(VDF-TrFE) films and implantable artificial cochlea were no cytotoxic effects on cultured neurons. The results presented here would provide the useful suggestions for further development of artificial organs research.

Acknowledgements

The authors would like to thank Dr. Yoichi Kagaya, Mr. Yohei Nakamoto, and Mr. Toshiya Kanbe, Graduate School of Engineering Science, Osaka University, for their technical support.

References

(1) Lewandowski, B.E., Kilgore, K.L., and Gustafson, K.J., Design considerations for an implantable, muscle powered piezoelectric system for generating electrical power, *Annals of Biomedical Engineering*, Vol. 35, No. 4 (2007), pp.631-641.

(2) Platt, S.R., Farritor, S., Garvin, K., and Haider, H., The use of piezoelectric ceramics for electric power generation within orthopedic implants, *IEEE/ASME Transactions on Mechatronics*, Vol. 10, No.4 (2005), pp.455-461.

(3) Schubert, W., Baurschmidt, P., Nagel, J., Thull, R., and Schaldach, M., An implantable artificial pancreas, *Medical & Biological Engineering & Computing*, Vol. 18, No. 4 (1980), pp. 527-537.

(4) Schrag, H.J., Ruthmann, O., Doll, A., Goldschmidtböing, F., Woias, P., and Hopt, U.T., Development of a novel remote-controlled artificial bowel sphincter through microsystems technology, *Artificial Organs*, Vol. 30, No. 11 (2006), pp. 855-862.

(5) Shintaku, H., Tanujaya, H., Nakamoto, Y., Nakagawa, T., Kawano, S., and Ito, J., Fluid dynamical analysis on basic characteristics of MEMS fabricated artificial cochlea," *The Seventh JSME-KSME Thermal and Fluids Engineering Conference*, (2008), p.155 & CDROM.

(6) Shintaku, H., Tanujaya, H., Nakagawa, T., Ito, J., and Kawano, S., Acoustical frequency selectivity of piezoelectric artificial cochlea, *Proceedings of the 25th Sensor Symposium on Seonsors, Micromachines, and Applied Systems*, (2008), pp.847-848.

(7) Shintaku, H., Nakagawa, T., Kanbe, T., Tanujaya, H., Kawano, S., and Ito, J., Microfabricated acoustic sensor with frequency selectivity and electric signal conversion for novel artificial cochlear system, will be presented at *2009 JSME-IIP/ASME-ISPS Joint Conference on Micromechatronics for Information and Precision Equipment (MIPE 2009)* (2009), pp. 341-342.

(8) Spelman, F.A., The past, present, and future of cochlear prostheses, *IEEE Engineering in Medicine and Biology Magazine*, Vol. 18, No. 3 (1999), pp. 27-33.

(9) Zeng, F.G., Trends in cochlear implants, *Trends in Amplification*, Vol. 8, No. 1 (2004), pp. T1–T34.

(10) Waltzman, S.B., Cochlear implants: current status, *Expert Review of Medical Devices*, Vol. 3, No. 5 (2006), pp. 647–655.

(11) Kotzar, G., Freas, M., Abel, P., Fleischman, A., Roy, S., Zorman, C., Moran, J.M., and Melzak, J., Evaluation of MEMS materials of construction for implantable medical devices, *Biomaterials*, Vol. 23, No. 13 (2002), pp. 2737-2750.

(12) Yamada, K.M., and Olden, K., Fibronectins-adhesive glycoproteins of cell surface and blood, *Nature*, Vol. 275, No. 5677 (1978), pp. 179-184.

(13) Kleinman, H.K., Klebe, R.J., and Martin, G.R., Role of collagenous matrices in the adhesion and growth of cells, *The Journal of Cell Biology*, Vol. 88, No.3 (1981), pp. 473-485.

(14) Muramoto, K., Kobayashi, K., Nakanishi, S., Matsuda, Y., and Kuroda, Y., Functional synapse formation between cultured neurons of rat cerebral cortex, *Proceedings of the Japan Academy Series B*, Vol. 64, No. 10 (1988), pp.319-322.

(15) Quinn, B., Toga, A.W., Motamed, S., and Merlic, C.A., Fluoro Nissl Green: a novel fluorescent counterstain for neuroanatomy, *Neuroscience Letters*, Vol. 184, No. 3 (1995), pp. 169-172.

(16) Ostuni, E., Kane, R., Chen, C.S., Ingber, D.E., and Whitesides, G.M., Patterning mammalian cells using elastomeric membranes, *Langmuir*, Vol.16, No. 20 (2000), pp. 7811-7819.

JOHNS
特集●耳の奇形●

症状・診断

内耳奇形の聴覚検査所見

熊川孝三*
Kozo KUMAKAWA

● Key Words ●内耳奇形，前庭水管拡大症，内耳道狭窄症●

はじめに

骨迷路の形態異常を伴う内耳奇形の頻度は一般に考えられているよりも高く，Jensen[1]は先天性高度感音難聴者の20％に認められると報告している。その分類には多くのものがある。

病理組織学的には，

1）Michel型：内耳の完全欠損
2）Mondini型：骨迷路，膜迷路が不完全に発育
3）Bing-Siebenmann型：骨迷路は正常で膜迷路，感覚細胞が不完全に発育
4）Scheibe型：蝸牛の膜迷路と球形嚢に障害があるが前庭膜迷路と骨迷路は正常に発育

などと分類されることが多い。しかし，このような分類は病理組織学的検査によって初めて可能になるもので，実際の画像・臨床診断には適さない。

そこでJackler ら[2]はこれらの点を考慮して**表1**のような分類を提唱している。これは，まず，膜迷路に限局した奇形と，骨迷路と膜迷路の異常を合併するものに大きく分け，さらに後者を，

A：内耳の無形成
B：蝸牛奇形を伴うもの
C：蝸牛の異常を伴わず半規管・前庭の迷路奇形のみを伴うもの
D：水管の奇形
E：内耳道の奇形

とに分ける分類である。これらの分類は画像診断の所見に基づいており，臨床診断に適している。ここではこの分類にしたがって内耳奇形を分類し，それぞれの聴覚検査所見について述べる。

表1　内耳奇形の分類（Jackler ら）[2]

Ⅰ．膜迷路に限局した奇形
　A．膜迷路の完全異形成
　B．膜迷路の限局した異形成
　　1）蝸牛，球形嚢の異形成（Scheibe）
　　2）蝸牛基底回転の異形成（Alexander）
Ⅱ．骨迷路と膜迷路の奇形
　A．迷路の無形成（Michel）
　B．蝸牛の奇形
　　1）蝸牛の無形成
　　2）蝸牛の低形成
　　3）骨隔壁の低形成（Mondini）
　　4）共通腔（common cavity）
　C．迷路奇形
　　1）半規管異形成
　　2）半規管無形成
　D．水管の奇形
　　1）前庭水管拡大
　　2）蝸牛水管拡大
　E．内耳道の奇形
　　1）内耳道狭窄
　　2）内耳道拡大

Ⅰ．内耳奇形の型と聴力像

Jackler らの分類[2]にしたがって，彼らの聴力レベルの解析結果を**表2**に示す。**図1**は蝸牛の異常を伴う内耳奇形について，**図2**は蝸牛の異常を伴わない半規管・前庭の内耳奇形について，筆者[3]が改変し，それぞれ発達が停止した胎生時期順に示した。

Michel型は内耳の完全欠損であり，当然ながら聴力はスケールアウトである。

Bの蝸牛奇形を伴う群の中で最も頻度が高いものは，一般的にMondini型奇形と呼ばれている奇

* 虎の門病院耳鼻咽喉科・聴覚センター
〔〒105-8470 東京都港区虎ノ門2-2-2〕

表 2　内耳奇形の分類と平均聴力（Jackler ら）[2]

型	耳数	0～40	41～80	81～100	101～120	>120 dB *
A 内耳の完全欠損（Michel）	1	—	—	—	—	1
B 蝸牛奇形を伴うもの						
蝸牛・前庭が共通腔	19	1	6	—	3	9
蝸牛無形成	2	—	—	—	1	1
蝸牛低形成	11	6	3	1	—	1
蝸牛回転の隔壁欠損（Mondini）	41	7	15	4	7	8
C 蝸牛奇形を伴わないもの						
前庭・半規管の形成不全	7	5	—	1	1	—
D 前庭水管の拡大	17	7	4	4	2	—

＊ 500，1000，2000 Hz の平均聴力

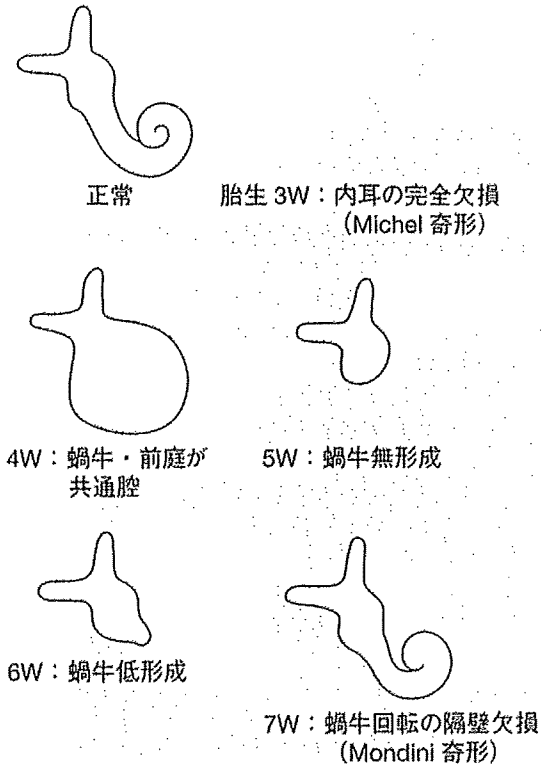

図 1　蝸牛の異常を伴う内耳奇形（Jackler[2] より改変）[3]
発達が停止した胎生時期を示す。

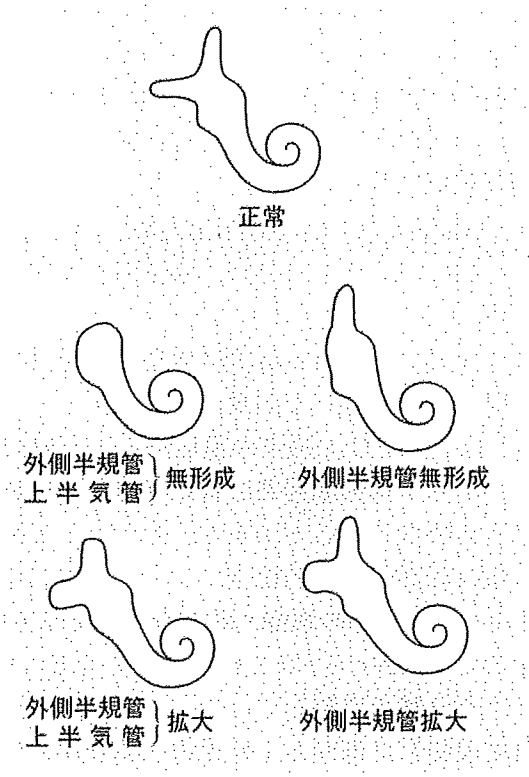

図 2　蝸牛の異常を伴わない内耳奇形（Jackler[2] より改変）[3]
胎生 6 週～22 週における発達の停止による。

形である。これは，胎生 7 週目の異常で，蝸牛軸が不完全で基底回転（第 1 回転）までは発達しているが，それよりも distal の回転間の隔壁が欠損し，中・頂回転が合わさって嚢状に置き換わったものである。コルチ器・有毛細胞と聴神経終末の欠損程度にはバラツキがあり，**表 2** に示したように難聴も軽度から高度までさまざまである。

次に多いのは胎生 4 週目の異常で，蝸牛と前庭が大きな共通した腔となって蝸牛の回転が形成されていない共通腔 common cavity 型と呼ばれているものである。聴力は表 2 に示すように不良なものが多いが，意外にも中等度の低下にとどまるものもある。

次いで，蝸牛低形成型では聴力低下は軽度のものが多いことがわかる。

C の蝸牛の異常を伴わない半規管・前庭の内耳

奇形は，表2に示したように，蝸牛形態が正常であるために，聴力低下も軽度なものが多いが，一方，高度な難聴を伴うこともある。

Dの前庭水管拡大を伴う奇形では聴力低下は軽度なものから高度まで幅広く分布し，変動性であり，また，低音域の気骨導差の存在が認められることが多い。このために聴力レベルの割に補聴効果が出やすいことが特徴的な点としてあげられる。

II．内耳奇形の型とラセン神経節の残存

内耳奇形でも型によってはラセン神経節がある程度数は形成されていることは組織学的にも確認されている。Jackler ら[4]は共通腔型の2耳，蝸牛低形成の2耳，Mondini 型奇形の1耳の計5耳に初めて単チャンネル方式人工内耳を埋め込み，音知覚を生ず得ることを確認した。以来，多チャンネル方式の人工内耳についても内耳奇形で有効であることが多数報告されている。

Schmidt[5]によれば，正常人のラセン神経節数は25,000から35,000であるのに対し，Mondini 型内耳奇形では7,677から16,110，平均11,478であったと報告している。さらにラセン神経節は共通腔奇形や蝸牛軸形成不全の奇形ではその耳胞壁に存在していると報告した。したがってこれらの内耳奇形でも必ずしも人工内耳が無効ではないと考えられる。ただし，周波数情報を十分に伝えるには，蝸牛の回転がある程度形成されている奇形，すなわちMondini型奇形の方が共通腔型奇形よりも聴取成績の点では有利であろう。Michel型奇形および蝸牛無形成の場合にはラセン神経節の形成もなく，人工内耳の適応とはならない。

III．前庭水管拡大症(Large vestibular aqueduct syndrome，以下LVASと略す)

1．概　説

1978年にValvassoriとClemis[6]によって報告された内耳奇形であり，内リンパ嚢と前庭水管の拡大を特徴とする。CT，MRIなど画像診断が先天性難聴児の画像診断に用いられるようになってから発見頻度は増え，内耳奇形の中でも最も頻度の高い奇形であるとされている[7]。

側頭骨の高分解能CTでは拡大した前庭水管が

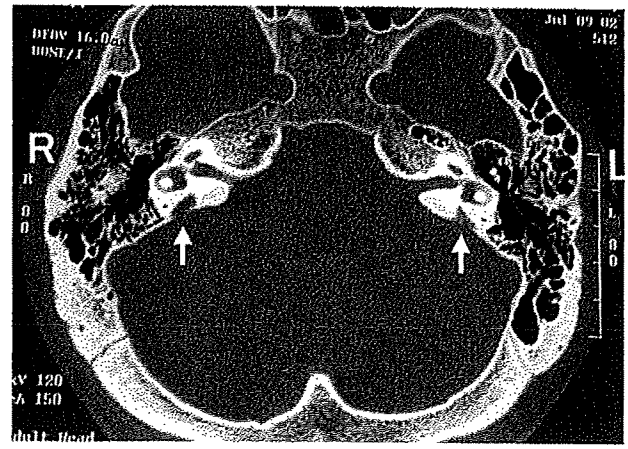

図3　前庭水管拡大症のCTスキャン
矢印：拡大した両側の前庭水管を示す。

前庭に直結している所見が認められる(図3)。合併する奇形として，半規管の異常，拡大した前庭，Mondini奇形の合併などがある。

2．症　状

小児期に発症して，時に頭部の外傷を契機として，めまい発作を反復しながら次第に進行し，ついには高度難聴となる難治性疾患として知られている。

3．遺伝学的異常

本疾患は常染色体劣性遺伝であり，Abe ら[8]は7番染色体長腕(7q31)に原因遺伝子が存在することを報告した。この領域は先天性感音難聴と甲状腺腫を伴うPendred症候群の原因遺伝子であるPDS遺伝子の存在する領域であるが，Usami ら[9]はPDS遺伝子が同時にLVASの原因遺伝子であることを明らかにし，両者はPDS遺伝子変異による表現型が異なる一連の疾患群であることを報告した。

4．聴覚検査所見

46～65％に小児期の難聴があり，15～25％に低音域の気骨導差の存在が認められるという[10]。低音域における気導骨導差の存在に対しては明白な機序は不明であるが，内リンパ圧の上昇によるアブミ骨の可動性の低下も一因として推測される。

内耳障害の機序としては拡大した前庭水管を通

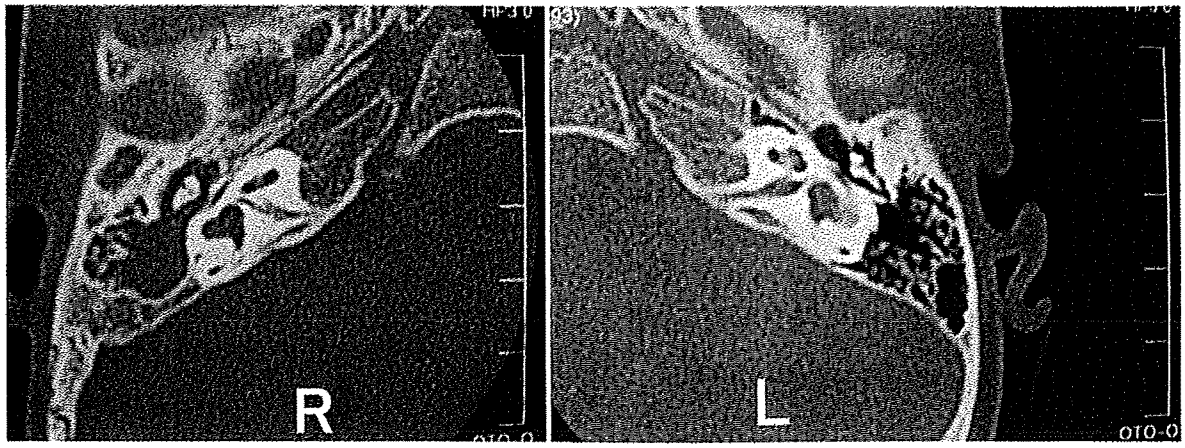

図 4　両側内耳道狭窄症の側頭骨 CT
右滲出液の貯留，外側半規管の奇形および両側内耳道の狭窄が認められる。

じて脳圧が内耳に伝わり，内耳の症状を誘発するものと考えられる。悪化に頭部外傷が契機となることはこれを裏付ける。時には膜迷路が破綻し，急激な聴力低下をきたし，最終的にはコルチ器の障害をきたすものと推測される。しかし，進行性の内耳障害をきたす他の因子の存在も否定できず，複数の機序が存在する可能性もある。

5．治　療

急性増悪時には突発性難聴に準じた副腎皮質ステロイド投与が行われ，ほとんどの例で奏効する。通常，1〜2 週間の投与で回復することが多い。しかし，頻回のめまい発作例では副作用のために投与を中止せざるを得ない例も多い。また長期的には次第に聴力が悪化するのを阻止できない場合が多く，最終的に人工内耳の適応となる例も多い。

これまでに LVAS 症例の拡大した内リンパ嚢を充填する手術が行われて，これを無効とする報告[10]と，有効とする Wilson ら[11]，内藤ら[12]の報告がある。

われわれは，乳突洞削開後に細い硬性内視鏡を硬膜と側頭骨の間に入れて空間を確保し，内リンパ嚢が側頭骨内に入ってゆく部位を確認し，そこでチタン製クリップを用いて内リンパ嚢をクリッピングする新しい術式を考案した[13,14]。本術式は内リンパ嚢の切開を行わずに済み，また圧迫による内リンパ圧の急激な上昇も避けられ，内耳に対する侵襲がこれまでの術式に比べて少なく，聴力保存については内リンパ嚢充填術よりも小侵襲のクリッピング術が有利であった。進行性に 80 dB 程度まで悪化し，かつ，保存治療で改善が期待できなくなった場合には外科的療法の 1 つとして試みられて良いと考える。

Ⅳ．内耳道奇形

1．概　説

ときに先天奇形あるいはクモ膜嚢胞による内耳道拡大が認められることがあるが，この場合，聴力は正常であることが多い。

先天性の内耳道狭窄は蝸牛前庭神経の形成不全が二次的に内耳道の狭窄を引き起こすと考えられている[15]。両側内耳道狭窄症は極めて稀である[16]。両側内耳道狭窄症例の側頭骨 CT を図 4 に示す。

2．内耳道狭窄症の聴覚検査所見

ほとんどの例で聴神経の低形成に伴う高度難聴が認められる。基本的に両側内耳道狭窄症は画像から診断がなされることがほとんどであり，最終的に人工内耳の適応決定，有効性予測の判断が問題となる。

画像診断で高度の両側内耳道狭窄症例あるいは内耳奇形が認められる症例に対して，われわれが行う聴覚検査ならびに画像診断のフローチャートを図 5 に示す。

BOA，CORの聴性行動反応検査，ABR，聴性定常反応検査（ASSR：auditory steady-state response）などの検査で聴覚反応がある程度認められた場合，一般的には純音聴力検査の閾値が100 dB未満で補聴器装用閾値が60 dB未満であれば補聴器の適応である。一方，高度難聴でも聴覚反応がわずかにあり，かつMRIで蝸牛神経が明らかに確認できれば，電気刺激ABR（EABR）を施行せずとも人工内耳適応ありとして問題ない。

しかし，聴覚反応がほとんどなく，さらにはMRIで聴神経が同定困難である場合には最終的には全身麻酔下で鼓膜から電極刺入し，これによる電気刺激ABR（electrically induced ABR：EABR）を行うことで適応を決定する。高橋，熊川ら[17]はEABRで反応が認められた両側内耳道狭窄症例に人工内耳埋め込み手術を行い，その有効性を報告した。

V．当院の高度難聴乳幼児の精密聴力検査システム

現在，難聴が疑われる乳児・幼児では，通常は聴性行動反応聴力検査（BOA），条件詮索反射聴力検査（COR），聴性脳幹反応検査（ABR）を行う。しかし行動観察方式の問題点として適応年齢，再現性，左右別の閾値測定が困難，重複障害児における正確さの問題がある。またABRの問題点としてクリック音を使うために低音域の聴力が反映されず，補聴器の装用効果を予測しにくいという難点がある。このため対象児の年齢が小さくなればなるほど，耳鼻咽喉科医は難聴の程度と聴力像の提示に難渋しているのが現状である。

また，画像検査も必要であり，各検査毎に通院と睡眠剤の投与を行うのは，患児，両親，医師のいずれにとっても負担であった。

そこで，われわれは乳幼児の精密聴力検査のシステムとして，周波数特性を持ち，かつ他覚的な聴力検査である蝸電図検査（electrocochleography：ECoG），聴性定常反応検査（ASSR）に加えて，岬角電気刺激によるEABRとCT，MRIも組み合わせて，短期間の入院で乳幼児の検査を効率的に行うシステムを考案し，同一小児群を対象にした検討で以下の結果を得た[18]。

1）鼓室内誘導法によるECoGとASSR検査を行うことでABR無反応耳の82％において低音域周波数の域値測定が可能となった。

2）鼓室内誘導法によるECoGはASSRよりも反応閾値は5～15 dB低く，その差は低音域ほど大きく，ECoGの反応検出率はASSRの2倍高かった。

3）EABRは聴覚反応の得られない内耳道狭窄例など蝸牛神経の形成不全が考えられる例ではきわめて有効な人工内耳の適応決定手段と考えられた。

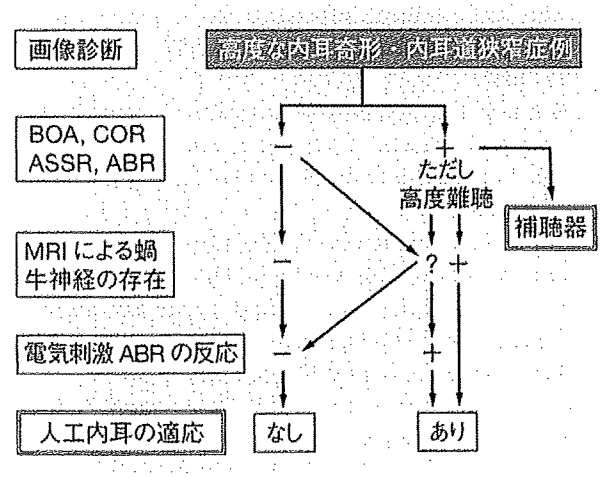

図 5　高度な内耳奇形・内耳道狭窄症の検査フローチャート

おわりに

内耳奇形の診断には聴覚検査のみならず，画像検査，遺伝学的検査も併せて行い，EABR検査が人工内耳の適応と有効性を予測する上で有用であることを述べた。

本研究は平成20年度厚生労働科学研究費補助金によって行われた。

文　献

1) Jensen J：Malformation of the inner ear in deaf children. Acta Radio (Suppl 286)：1-97, 1969.
2) Jackler RK, Luxford WM, House WF：Congenital malformation of the inner ear；A classification based on embryogenesis. Laryngoscope 97 (Suppl 40)：2-14, 1987.
3) 熊川孝三：幼少児難聴の画像診断―内耳奇形と人工内耳―．耳鼻と臨床 40：95-99，1994.
4) Jackler RK, Luxford WM, House WF：Sound detec-

tion with cochlear implant in five cases of four children of the cochlea. Laryngoscope 97 (suppl 40) : 15-17, 1987.
5) Schmidt JM : Cochlear neuronal populations in developmental defects of the inner ear ; Implications for cochlear implantation. Acta Oto-Laryngologica 99 : 14-20, 1985.
6) Valvassori GE, Clemis JD : The large vestibular aqueduct syndrome. Laryngoscope 88 : 723-748, 1978.
7) Smith SD, Harker LA : Single gene influences on radiologically-detectable malformations of the inner ear. J Commun Disord 31 : 391-410, 1998.
8) Abe S, Usami S, Shinkawa H : Three familial cases of hearing loss associated with enlarged vestibular-aqueduct maps to 7q31, the region containing the Pendred gene. Am J Med Genet 82 : 322-328, 1999.
9) Usami S, Abe S, Weston MD, et al : Non-syndromic loss associated with enlarged vestibular aqueduct is caused by PDS mutations. Hum Genet 104 : 188-192, 1999.
10) Zalzal GH, Thomaski SM, Vezina LG, et al : Enlarged vestibular aqueduct and sensorinueral hearing loss in childhood. Arch Otolarungol Head Nech Surg 121 : 23-28, 1995.
11) Wilson DF, et al : Endolymphatic sac obliteration for large vestibular aqueduct syndrome. Am J Otol 18 : 101-107, 1997.
12) 内藤　泰，高橋晴雄：前庭水管の手術について．耳鼻臨床 93：802-803，2000.
13) 熊川孝三，高橋優宏，武田英彦，他：前庭水管拡大症に対する内視鏡使用による内リンパ嚢クリッピング術．Otol Jpn 13：251，2003.
14) 熊川孝三，宇佐美真一：前庭水管拡大症．JOHNS 21 (9)：1199-1201，2005.
15) Nelson EG, Hinojosa R : Aplasia of the cochlear nerve ; A temporal bone study. Otol Neurotol 22 : 790-795, 2001.
16) Camacho RR, Berrocal JRG, Arellano B : Bilateral malformation of the internal auditory canal ; Atresia and contralateral transeverse megacrest. Otolaryngol Head Neck Surg 125 : 115-116, 2001.
17) 高橋優宏，熊川孝三，武田英彦，他：人工内耳埋め込みが有効であった両側内耳道狭窄頭の1症例．Otol Japan 14：248-251，2004.
18) 熊川孝三，鈴木久美子，武田英彦，他：短期入院による乳幼児の他覚的精密聴力検査―システムの紹介およびABR，蝸電図，聴性定常反応，EABRの検討―．Audiology Japan 48：156-164，2005.

*　　*　　*

Pflugers Arch - Eur J Physiol (2009) 457:885–898
DOI 10.1007/s00424-008-0560-z

SENSORY PHYSIOLOGY

Immune atomic force microscopy of prestin-transfected CHO cells using quantum dots

Michio Murakoshi · Koji Iida · Shun Kumano · Hiroshi Wada

Received: 22 April 2008 / Revised: 7 July 2008 / Accepted: 14 July 2008 / Published online: 2 August 2008

Abstract Prestin, a membrane protein of the outer hair cells (OHCs), is known to be the motor which drives OHC somatic electromotility. Electron microscopic studies showed the lateral membrane of the OHCs to be densely covered with 10-nm particles, they being believed to be a motor protein. Imaging by atomic force microscopy (AFM) of prestin-transfected Chinese hamster ovary (CHO) cells revealed 8- to 12-nm particle-like structures to possibly be prestin. However, since there are many kinds of intrinsic membrane proteins other than prestin in the plasma membranes of OHCs and CHO cells, it was impossible to clarify which structures observed in such membranes were prestin. In the present study, an experimental approach combining AFM with quantum dots (Qdots), used as topographic surface markers, was carried out to detect individual prestin molecules. The inside-out plasma membranes were isolated from the prestin-transfected and untransfected CHO cells. Such membranes were then incubated with antiprestin primary antibodies and Qdot-conjugated secondary antibodies. Fluorescence labeling of the prestin-transfected CHO cells but not of the untransfected CHO cells was confirmed. The membranes were subsequently scanned by AFM, and Qdots were clearly seen in the prestin-transfected CHO cells. Ring-like structures, each with four peaks and one valley at its center, were observed in the vicinity of the Qdots, suggesting that these structures are prestin expressed in the plasma membranes of the prestin-transfected CHO cells.

M. Murakoshi · K. Iida · S. Kumano · H. Wada (✉)
Department of Bioengineering and Robotics, Tohoku University,
6-6-01 Aoba-yama,
Sendai 980-8579, Japan
e-mail: wada@cc.mech.tohoku.ac.jp

Keywords Auditory system · Cochlea · Hair cell · Membrane · Motor systems · Imaging · Microscopy

Introduction

The high sensitivity, sharp frequency selectivity, and wide dynamic range of mammalian hearing are achieved by cochlear amplification, the mechanism of which is realized due to outer hair cell (OHC) somatic motility [1–4], operating at up to microsecond rates [5]. This motility was thought to be associated with a membrane protein in the lateral wall of OHCs [6], but was later found to be realized by the motor protein prestin [7].

Prestin consists of 744 amino acid residues with a molecular weight of around 81.4 kDa. Hydrophobicity analysis indicated that prestin has two large protruding fragments, i.e., N (approximately 100 amino acids [a.a.]) and C termini (approximately 250 a.a.), extending into the cytoplasm and a hydrophobic center core (approximately 400 a.a.) with 12 transmembrane domains [8]. Later, however, it was clarified that two of these domains do not penetrate the plasma membrane [9]. On the other hand, a prestin topology with 10 transmembrane domains has also been reported [10]. Among these termini, the STAS (after sulfate transporter and antisigma factor antagonist) domain (amino acids 525–713; molecular weight of 21 kDa), located at the C terminus of prestin [5], possibly occupies a large portion of the conformational space of the cytoplasmic region. Homooligomerization of prestin has been reported to be a tetramer [11, 12] and its N terminus is possibly important for this conformation [10].

Previous morphological studies of OHCs using an electron microscope have shown the lateral membrane of the OHCs to be densely covered with particles about 10 nm

in diameter, these particles being believed to be a motor protein [13–16]. The lateral membrane has also been observed by atomic force microscopy (AFM) and the existence of many particles with diameters of about 10 nm has also been reported [17]. Imaging by AFM of prestin-transfected Chinese hamster ovary (CHO) cells has revealed that particle-like structures 8–12 nm in diameter are possibly prestin [18]. However, since there are many kinds of intrinsic membrane proteins other than prestin in the plasma membranes of OHCs and CHO cells, it was impossible to clarify which structures observed in such membranes were prestin. More recently, prestin has been reported to be expressed in insect cells and has been purified from these cells. Using such purified prestin, its 3-D structure was clarified to be a bullet-shaped particle by transmission electron microscopy (TEM) [12]. However, the structure of purified prestin is not necessarily identical to that of prestin expressed in the native cell plasma membrane. In addition, TEM-based analysis of the protein structure requires time-consuming and cumbersome techniques for sample preparation to obtain a sufficient amount of purified protein for experimentation.

In the present study, an experimental approach combining AFM with quantum dots (Qdots), used as topographic surface markers, was employed to detect individual prestin molecules. The inside-out plasma membranes were isolated from the prestin-transfected and untransfected CHO cells. Such membranes were then incubated with antiprestin primary antibodies and Qdot-conjugated secondary antibodies. The plasma membranes of both types of CHO cells were subsequently observed by fluorescence microscopy and then scanned by AFM.

Materials and methods

Cells and cell culture

Prestin-transfected and untransfected CHO cells were used. The prestin-transfected CHO cells were constructed by transfection of gerbil prestin cDNA into CHO cells using pIRES-hrGFP-1a mammalian expression vectors (Stratagene, La Jolla, CA, USA). Those expression vectors contain humanized *Renilla reniformis* green fluorescent protein (hrGFP) gene and the GFP is expressed in the cytoplasm of the cells. CHO cell lines, which stably express prestin, were established using transfected cells by limiting dilution cloning. The expression and activity of prestin in the generated CHO cell lines were confirmed by immunofluorescence and whole-cell patch clamp measurements [19, 20]. CHO cells, which were not subjected to any transfection procedure, were used as the untransfected CHO cells.

The prestin-transfected and untransfected CHO cells were cultured in RPMI-1640 medium with 10% fetal bovine serum, 100 U penicillin/ml, and 100 μg streptomycin/ml at 37°C with 5% CO_2. At the beginning of every experimental procedure, the GFP fluorescence of the prestin-transfected CHO cells were observed by using a confocal laser scanning microscope (FV500, Olympus, Tokyo, Japan) equipped with a UPlan Apo ×20 (NA=0.70) objective and an Ar laser (488 nm) to confirm the expression of prestin.

Isolation of plasma membranes

The inside-out plasma membranes, i.e., cytoplasmic face is up, were isolated from the prestin-transfected CHO cells as described elsewhere [21]. The culture medium was removed and the cells were detached from a flask by incubation with 100 μM ethylenediamine tetraacetic acid (EDTA) in phosphate buffered saline (PBS) solution for 5 min at 37°C. The EDTA–PBS solution containing the cells was put into a tube and centrifuged at 250×*g* for 5 min. The supernatant was then removed and the culture medium was put into the tube. The culture medium containing the cells was agitated by pipetting in that tube and deposited on glass-bottomed dishes (Asahi Techno Glass, Chiba, Japan). After overnight culture, most of the cells had become reattached and spindle-shaped on the substrate. The culture medium was discarded and the cells were washed twice with an external solution (145 mM NaCl, 5.8 mM KCl, 1.3 mM $CaCl_2$, 0.9 mM $MgCl_2$, 10 mM HEPES, 0.7 mM Na_2HPO_4, and 5.6 mM glucose; pH 7.3) warmed to 37°C for removal of unwanted materials, such as cell fragments and proteins contained in the culture medium attached to the surfaces of the cells and substrate. The dish was immersed for 3 min in a hypotonic buffer (10 mM piperazine-*N*,*N*′-bis(2-ethanesulfonic acid), 10 mM $MgCl_2$, 0.5 mM ethylene glycol bis(2-aminoethyl ether)-*N*,*N*,*N*′,*N*′-tetraacetic acid; pH 7.2), which had been cooled to 4°C. The cells were then sheared open by gentle exposure to a stream of the hypotonic buffer using a 1-ml pipette (Gilson, Villiers, France) several times, resulting in the isolation of the inside-out basal plasma membranes. After the isolated plasma membranes had been washed with PBS three times, they were incubated with a high-salt buffer (2 M NaCl, 2.7 mM KCl, 1.5 mM KH_2PO_4, 1 mM Na_2HPO_4; pH 7.2) for 30 min at room temperature to remove the cytoskeletal materials and the peripheral proteins [22]. The isolated membranes were then incubated with 0.05% trypsin for 1 min at room temperature to remove the remaining materials.

Sample preparation for prestin labeling with Qdots and AFM imaging

The isolated plasma membranes were fixed with 4% paraformaldehyde in PBS for 30 min at room temperature.

After fixation, the membranes were rinsed three times with PBS and incubated with Block Ace (Dainippon Pharmaceutical, Osaka, Japan) for 30 min at 37°C. After PBS washing, the membranes were incubated with goat antiprestin N terminus primary antibody (Santa Cruz Biotechnology, Santa Cruz, CA, USA) at a dilution of 1:100 in PBS overnight at 4°C. The membranes were then washed with PBS and incubated with Qdot® 655-conjugated rabbit antigoat IgG secondary antibody (Invitrogen, Carlsbad, CA, USA) at a dilution of 1:200 in PBS for 60 min at 37°C. Finally, the membranes were washed with Hanks' balanced salt solution (HBSS; 5.33 mM KCl, 0.44 mM KH_2PO_4, 137.93 mM NaCl, 0.34 mM Na_2HPO_4, 0.56 mM glucose; pH 7.3) and immersed in this solution filtered with a 0.22-μm pore-size syringe filter (Millipore, Billerica, MA, USA).

Fluorescence microscopy

Fluorescence images were obtained from the isolated membranes of the prestin-transfected CHO cells and those of the untransfected CHO cells by an inverted fluorescence microscope equipped with a Plan Apo ×100 (NA=1.40) oil immersion objective and a cooled CCD camera (DP70, Olympus), which comprised a part of the AFM used in this study, the exposure time being 2 s. This system enables simultaneous recording of fluorescence and AFM images of the same sample. A mercury lamp was used as a light source. Qdot fluorescence was detected with a wide-band filter cube (U-MWIG, Olympus) composed of a 520- to 550-nm excitation filter, a 565-nm dichroic mirror, and a 580-nm emission filter.

Atomic force microscopy

An AFM (NVB100, Olympus), in which the AFM unit is mounted on an inverted fluorescence microscope (IX70, Olympus), was used, such mounting making it easy to position the tip above the cells. This AFM is controlled by NanoScope IIIa (Digital Instruments, Santa Barbara, CA, USA; software version, v4.23). A V-shaped silicon nitride cantilever (OMCL-TR400PSA-2, Olympus) with a spring constant of 0.02 N/m was used. The cantilever has a pyramidal tip, the typical radius of its curvature being 16± 1 nm (personal communication with Olympus). To minimize sample damage during scanning, AFM images were obtained using the oscillation imaging mode (Tapping mode™, Digital Instruments). The cantilever was oscillated near its resonance frequency in liquid (3.6–4.7 kHz). Low- (60.0×60.0 μm), middle- (11.7×11.7 μm), and high-magnification images (2.3×2.3 μm) were obtained at a scan rate of 1.0 Hz, i.e., the scan speeds were 120, 23.4, and 4.6 μm/s, respectively. By scanning the sample with this mode, the height and phase images of the sample surface were obtained. The phase image was constructed by monitoring the phase lag between the input signal to the cantilever (i.e., driving signal used to drive the cantilever at its resonance for tapping mode, a sinusoidal signal of 3.6–4.7 kHz in this study) and the output signal from the cantilever detected by the laser system of the AFM (i.e., detected signal from the photodiode detector). For all AFM images, the samples were scanned from left to right. Each scan line had 512 points of data and an image consisted of 512 scan lines.

Analysis of AFM images

The original AFM images were flattened by use of a software program (NanoScope v4.23, Digital Instruments) to eliminate background slopes and to correct dispersions of individual scanning lines. AFM images were generated by raster scanning with a cantilever across a sample, i.e., left to right and top to bottom in a zigzag pattern. During this scanning, the topological data were continuously obtained in the transversal direction of the AFM image, i.e., left to right of the image, while such data in the longitudinal direction, i.e., top to down of the image, were intermittent. Thus, the topological data in the transversal direction of the image were more reliable than those in the longitudinal direction. The transversal sizes of the observed structures were, therefore, measured.

In the present study, Qdots were used as topographic surface markers. As the prestin molecules were labeled with primary and secondary antibodies, the distance between a Qdot and a prestin molecule was estimated to be approximately 20 nm [23]. The primary antibody used in this study reacts with the cytoplasmic N terminus of prestin. Since such terminus consists of approximately 100 a.a., its length was estimated to be approximately 31 nm [24]. Assuming that the antibody binds to the tip of the N terminus, the estimated maximum distance between a Qdot and the transmembrane domain of a prestin molecule is approximately 50 nm. Due to the architecture of the AFM system used in the present study, a 133-nm square AFM image containing one Qdot at its center was obtained by applying cubic spline interpolation to a high-magnification AFM image. All structures observed within 66.5 nm apart from the center of the Qdot were subjected to subsequent size analysis.

The diameter of the observed structure was estimated using a simple geometric model since such sizes are prone to overestimation due to the radius of the curvature of the AFM tip [25]. The relationship between the diameter of the structure observed by the AFM (2Δ) and its actual diameter ($2r$) is given by:

$$2\Delta = 2\left\{(R+r)^2-(R+H/2)^2\right\}^{1/2} \quad (1)$$

where R is the radius of the curvature of the AFM tip and H is the thickness of the plasma membrane, as described in

our previous study [18]. In the present study, R and H were considered to be the same as those of the previous study, i.e., 16 and 5 nm, respectively. When the observed structure was ring-like, the distance between two peak heights based on the cross sections was measured and was regarded as being its diameter.

Image analysis was performed with NanoScope v7.00 (Veeco, Santa Barbara, CA, USA) and data analyses, i.e., statistical analysis and Gaussian fit, were performed with IGOR Pro v6.0.3 (WaveMetrics, Lake Oswego, OR, USA). The Gaussian fit is given by:

$$f(x) = y_0 + A\exp\left\{(x - x_0)^2/(x_{width})^2\right\} \quad (2)$$

where y_0 is the base line, A is the amplitude, x_0 is the estimated peak position, and x_{width} is the full width at half maximum of the fitting curve.

Observation by AFM of Qdots on mica

Freshly cleaved mica was incubated with 50 μl of 0.5% (*w/v*) poly-L-lysine (MW=1,000–4,000; Sigma-Aldrich, St. Louis, MO, USA) in PBS. After 1 min adsorption, the mica was washed with Mill-Q water three times and dried at room temperature. Then, Qdots were prepared in PBS at a dilution of 1:1,000. A 100-μl solution of Qdots was deposited on the poly-L-lysine-coated mica and allowed to adsorb for 20 min. The supernatant was then removed and the mica was rinsed gently with 200 μl of Milli-Q water three times. After the sample was air-dried at room temperature, it was immediately imaged by AFM. To analyze the size and number of Qdots, first, the obtained image was converted into grayscale AFM images, the intensity value of which ranged from 0 (black) to 255 (white), by using Adobe Photoshop 6.0 (Adobe Systems, San Jose, CA, USA). The number of Qdots was counted by the command "Analyze particles" of ImageJ v1.32j (NIH, Bethesda, MD, USA) and their heights were then analyzed by the use of a command "section" of NanoScope v4.23. Every extracted structure was subjected to height analysis to prevent experimenter bias.

Results

Prestin labeling with Qdots and low-magnification AFM images

Evaluating the expression of prestin in the transfected CHO cells, the fluorescence of GFP, coexpressed with prestin in such cells, was observed since the GFP fluorescence is positively correlated with the expression of prestin in the prestin-transfected CHO cells [26]. Figure 1 shows the GFP fluorescence of the prestin-transfected and untransfected CHO cells. GFP fluorescence was detected in the prestin-transfected cells (top middle panel), indicating the expres-

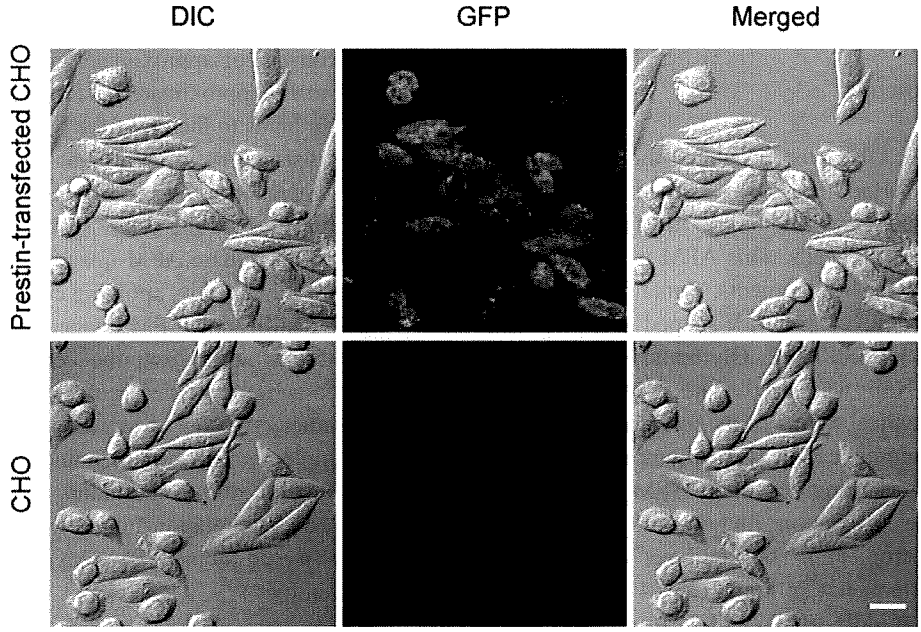

Fig. 1 GFP fluorescence of the prestin-transfected and untransfected CHO cells. *Left panels* differential interference contrast (*DIC*) images, *middle panels* GFP fluorescence images, *right panels* merged images. GFP fluorescence was detected in the prestin-transfected cells (*top middle panel*), indicating the expression of prestin in the cells. By contrast, GFP fluorescence was not observed in the untransfected CHO cells (*bottom middle panel*). Scale bar is 20 μm

sion of prestin in the cells. By contrast, GFP fluorescence was not observed in the untransfected CHO cells (bottom middle panel).

Figure 2a shows the prestin labeling with Qdots and the corresponding low-magnification AFM images of the isolated plasma membranes of a prestin-transfected CHO cell and those of an untransfected CHO cell. Prestin labeling (red), which labels the N terminus of prestin, was observed in the isolated plasma membrane of the prestin-transfected CHO cell (top left panel); by contrast, it was not observed in the isolated plasma membrane of the untransfected CHO cell (top right panel). These results indicate the presence of prestin in the isolated plasma membranes of the prestin-transfected CHO cell even after the plasma membranes were isolated by gentle exposure to the hypotonic buffer and incubated with the high-salt buffer and trypsin. Low-magnification AFM images are shown in the bottom panels in Fig. 2a. The surface topologies of

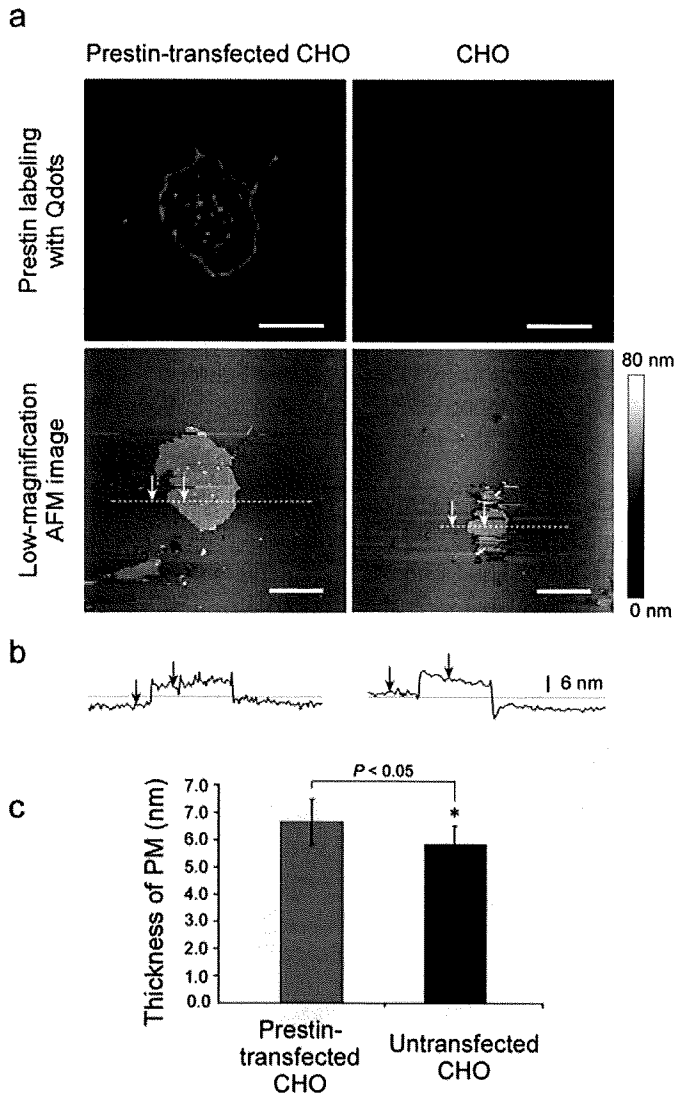

Fig. 2 Isolated plasma membranes of the prestin-transfected and untransfected CHO cells. **a** Fluorescence images of prestin labeled with Qdots and the corresponding low-magnification AFM images. Prestin labeling (*red*), which labels the N terminus of prestin, was observed in the isolated plasma membrane of the prestin-transfected CHO cell, but not observed in the isolated plasma membrane of the untransfected CHO cell. Low-magnification AFM images indicated that the surface topologies of the cytoplasmic faces of the prestin-transfected and untransfected CHO cells were flat at this magnification. Scale bars are 10 μm. **b** The cross sections of the isolated plasma membranes along the *dotted line* shown in the *bottom panels* of **a**. Height difference between the *arrows*, each horizontal distance of which was 6 μm, was measured as the thickness of the isolated plasma membrane. **c** Mean and standard deviation of the thickness of the isolated plasma membranes. The average thickness of the isolated plasma membranes of the prestin-transfected CHO cells was 6.65± 0.83 nm (n=16) and that of the untransfected CHO cells was 5.83± 0.67 nm (n=9). The thickness of the isolated plasma membranes showed statistically significant difference between the prestin-transfected and untransfected CHO cells, as indicated by the *asterisk* (P< 0.05, Student's t test)

the cytoplasmic faces of both prestin-transfected and untransfected CHO cells seem to be flat at this magnification. Figure 2b shows the cross sections of the isolated plasma membranes along the dotted line shown in the bottom panels of Fig. 2a. Height difference between the arrows shown in the figures, each horizontal distance of which was 6 μm, was measured as the thickness of the isolated plasma membrane. The mean and standard deviation of the thickness of the different isolated plasma membranes of the prestin-transfected and untransfected CHO cells are shown in Fig. 2c. The average thickness of the isolated plasma membranes of the prestin-transfected CHO cells was 6.65±0.83 nm (n=16) and that of the untransfected CHO cells was 5.83±0.67 nm (n=9). The thickness of the isolated plasma membrane showed statistically significant difference between the prestin-transfected and untransfected CHO cells, as indicated by the asterisk (P<0.05, Student's t test).

Low-, middle-, and high-magnification AFM images

The cytoplasmic surfaces of the isolated plasma membranes of the prestin-transfected CHO cells and those of the untransfected CHO cells were observed by the tapping mode of AFM.

Figure 3 is a fluorescence image of prestin labeled with Qdots in the prestin-transfected CHO cell (Fig. 3a) and the corresponding AFM images at low- (Fig. 3b) and middle-magnifications (Fig. 3c). The inset in each image is the digital zoom of the boxed area in each image. The middle-magnification image (Fig. 3c) was obtained from the boxed area in Fig. 3b. As shown in Fig. 3a, the distribution of prestin labeling with Qdots in the plasma membrane of the prestin-transfected CHO cell was seen as a pattern of bright patches, as indicated by the arrowheads in its inset. The fluorescence of Qdots in the area surrounding the patches but not in the substrate area (asterisk, Fig. 3a) was also observed although its intensity was weak, indicating that prestin is nonuniformly distributed all over the plasma membrane of CHO cells. In the low-magnification AFM image (Fig. 3b), the smooth surface of the cytoplasmic face of prestin-transfected CHO cells was confirmed. However, as shown in its digital-zoomed image (inset, Fig. 3b), bulges about 7 nm in height were observed, as shown by the arrowheads. Comparison between the digital-zoomed images of Fig. 3a and b reveals that the location of the bright patches of Qdot labeling and the bulges are colocalized. Furthermore, by comparing the digital-zoomed image of Fig. 3b with c, the bulges seen in Fig. 3b (dotted circles) corresponded to the small bumps seen in Fig. 3c (dotted circles).

Figure 4 shows the high-magnification AFM images of the boxed area of Fig. 3c. In these images, particles about 8 nm in height were observed as shown by the arrows. No changes in the location of these particles were observed between the scanning from the top to the bottom (Fig. 4a) and the subsequent scanning from the bottom to the top (Fig. 4b).

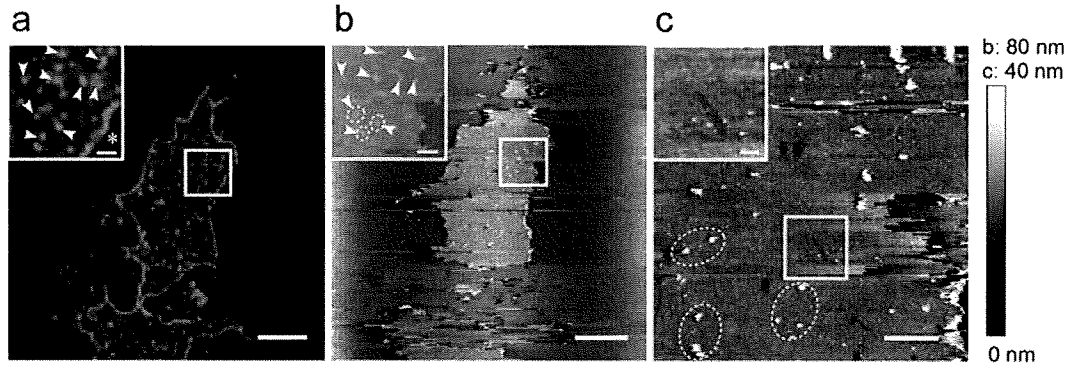

Fig. 3 Fluorescence image of prestin labeled with Qdots and the corresponding AFM images of the prestin-transfected CHO cell. **a** Fluorescence image of prestin labeled with Qdots. The *inset* shows a digital-zoomed image of the *boxed area*. **b** AFM image at low magnification. The *inset* is the digital zoom of the *boxed area*. **c** Middle-magnification AFM image obtained from the *boxed area* shown in **b**. The *inset* shows the digital zoom of the *boxed area*. As shown in **a**, the distribution of prestin labeling with Qdots in the plasma membrane of the prestin-transfected CHO cell was seen as a pattern of bright patches, as indicated by the *arrowheads* in its *inset*. As well as from such bright patches, fluorescence of Qdots was also detected from all over the plasma membrane while it was not observed in the substrate area (*asterisk*), indicating that prestin was nonuniformly distributed all over the plasma membrane of CHO cells. In the low-magnification AFM image (**b**), the smooth surface of the cytoplasmic face of prestin-transfected CHO cells was confirmed. However, as shown in its digital-zoomed image, the bulges about 7 nm in height were observed, as shown by the *arrowheads* in its *inset*. Comparison between the digital-zoomed images of **a** and **b** revealed that the location of the bright patches of Qdot labeling and the bulges were colocalized. Furthermore, by comparing the digital-zoomed image of **b** with **c**, the bulges indicated by *dotted circles* in **b** were found to correspond to the small bumps indicated by *dotted circles* in **c**. Scale bars of **a**, **b**, and **c** are 10, 10, and 2 μm, respectively. Scale bars of the insets of **a**, **b**, and **c** are 2 μm, 2 μm, and 500 nm, respectively

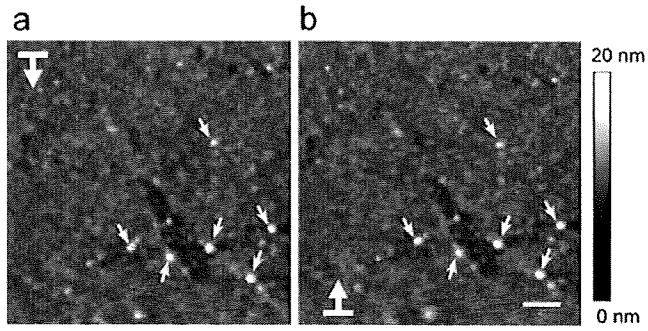

Fig. 4 High-magnification AFM images of the *boxed area* of Fig. 3c. **a** Image obtained by scanning from the top to the bottom of the sample. **b** Image obtained by scanning from the bottom to the top of the sample. In these images, particles about 8 nm in height were observed, as indicated by the *arrows*. No changes in the location of these particles were observed between **a** and **b**. Scale bar is 300 nm

Figure 5 indicates the AFM images of the isolated plasma membranes of the untransfected CHO cell at different magnifications. Low-, middle-, and high-magnification AFM images are shown by Fig. 5a,b, and c, respectively. The middle-magnification image (Fig. 5b) was obtained from the boxed area in Fig. 5a. The high-magnification image (Fig. 5c) was obtained from the boxed area in Fig. 5b. In the high-magnification image, although there are a few accumulations more than 15 nm in height, no other obvious structures are seen.

Observation by AFM of Qdots on mica and the plasma membrane

In this study, Qdots were used as topographic surface markers. To confirm the shape of Qdots, they were adsorbed on freshly cleaved mica coated with poly-L-lysine and immediately scanned by AFM. Figure 6a shows the Qdots adsorbed on mica. Uniform particles about 8 nm in height were observed. The frequency distribution of the Qdots on mica (red, n=45) is shown in Fig. 6b, along with such distribution of the Qdots observed on the plasma membranes of the prestin-transfected CHO cells (blue, n=78), which label prestin molecules due to an antigen–antibody reaction. This histogram exhibited Gaussian distributions for both data sets (red, y_0=0.6±2.2, A=9.6±2.3, x_{width}=0.7±0.2; blue, y_0=−2.1±7.5, A=8.2±7.1, x_{width}=2.9±2.2). The peaks of the Qdots observed on mica and on the isolated plasma membranes were 8.2±0.1 nm and 7.9±0.3 nm, respectively. The mean and standard deviations of the heights of Qdots observed on mica and the isolated plasma membranes are shown in Fig. 6c. The average height of the Qdots on mica was 8.2±0.5 nm and that observed on the plasma membranes of the prestin-transfected CHO cells was 7.9±1.3 nm. These two sizes of Qdots were statistically identical (P>0.05, Student's t test).

Figure 7a shows a high-magnification AFM height image of the isolated plasma membrane of the prestin-transfected CHO cell, the prestin molecules of which were labeled with Qdots. Different sizes of particles are observed in the height image. Figure 7b shows the phase image of a. Figure 7c indicates the cross sections of the phase images of particles A and B obtained between α and α′, and β and β′ (arrowheads), respectively. As shown in these figures, a bright phase contrast (positive phase shift) was observed at the center of particle B while a dark phase contrast (negative phase shift) was observed at its periphery. By contrast, such phase shifts were not observed for particle A.

Prestin topology in the isolated plasma membranes of CHO cells

Figure 8 shows high-magnification 3-D AFM images of a prestin-transfected CHO cell. Qdots 8 nm in height were clearly observed on the cytoplasmic face of the isolated plasma membrane of the prestin-transfected CHO cell, as indicated by black arrowheads. As shown in the magnification in the right of Fig. 8a, a ring-like structure with four

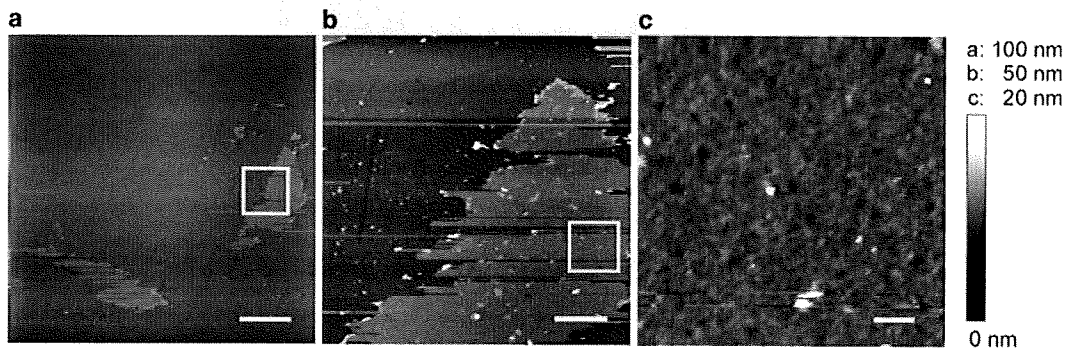

Fig. 5 AFM images of isolated plasma membranes of an untransfected CHO cell at different magnifications. **a** Low-magnification image. **b** Middle-magnification image obtained from the *boxed area* shown in **a**. **c** High-magnification image obtained from the *boxed area* shown in **b**. In the high-magnification image, although there are a few accumulations more than 15 nm in height, no other obvious structures are seen. Scale bars of **a**, **b**, and **c** are 10 μm, 2 μm, and 300 nm, respectively

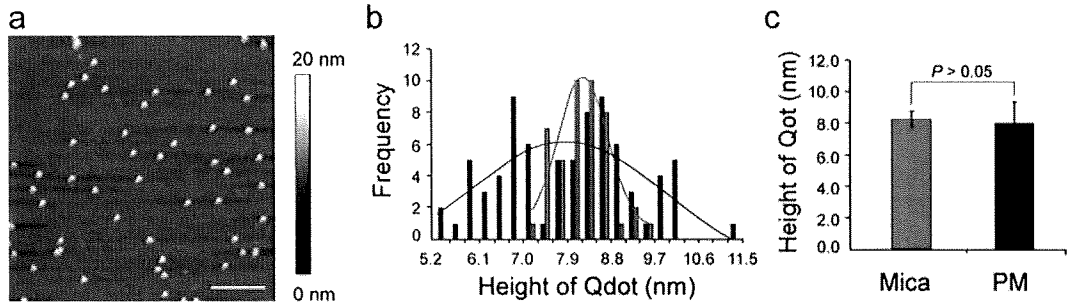

Fig. 6 The Qdots adsorbed on the freshly cleaved mica coated with poly-L-lysine. **a** AFM image. Uniform particles about 8 nm in height were observed. Scale bar is 200 nm. **b** Frequency distribution of the Qdots on mica and on the isolated plasma membranes of prestin-transfected CHO cells. *Red bars* show the frequency distribution of the Qdots on mica (n=45) and *blue bars* show such distribution of the Qdots on the plasma membranes of the prestin-transfected CHO cells, which label prestin molecules due to the antigen–antibody reaction (n=78). These histograms exhibited Gaussian distributions for both data sets, as shown by *red* and *blue lines* (red, y_0=0.6±2.2, A=9.6±2.3, x_{width}=0.7±0.2; blue, y_0=−2.1±7.5, A=8.2±7.1, x_{width}=2.9±2.2). The peaks of the former and the latter were 8.2±0.1 and 7.9±0.3 nm, respectively. **c** Mean and standard deviations of the heights of Qdots observed on mica and the isolated plasma membranes. The average height of the Qdots on mica was 8.2±0.5 nm and that observed on the plasma membranes of the prestin-transfected CHO cells was 7.9±1.3 nm. These two sizes of Qdots were statistically identical (P>0.05, Student's t test)

peaks and one valley at its center, possibly corresponding to a prestin molecule, was observed in the vicinity of the Qdot (A, arrow). In the vicinity of the other Qdots, similar structures were observed at the locations indicated by arrows (A–D), the magnifications of which are shown in the bottom panels.

Figure 8b shows examples of 3-D images of the structures observed in the vicinity of the Qdots. These images were obtained from the different cells shown in Fig. 8a. Most of the observed structures are ring-like structures with a depression surrounded by four peaks (E–K). In some cases, such structures are adjacent to the others, forming a unit with two molecules (L). Besides those ring-like structures, a square-shaped structure with a protrusion at its center, four corners of which are indicated by arrowheads, was also observed (M). The side length of the square, i.e., the length between the adjacent corners indicated by arrowheads, was 7.7 nm and the diameter of the protrusion was 6.2 nm, derived from Eq. 1.

Figure 8c indicates the frequency distribution of the diameter of the ring-like structures (n=120). In the present study, we observed the cytoplasmic faces of the plasma

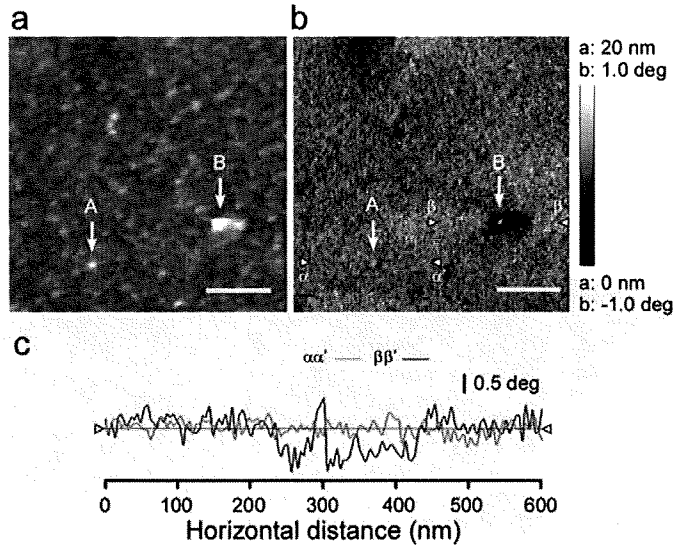

Fig. 7 Height and phase AFM images of the isolated plasma membrane of the prestin-transfected CHO cell incubated with antiprestin antibody and Qdot-conjugated secondary antibody. **a** High-magnification height image. Different sizes of particles are observed (*A* and *B*, *arrows*). **b** Phase image of **a**. **c** Cross sections of phase images of the particles *A* and *B* (between α and α' and β and β', *arrowheads*). Regarding particle *B*, a bright phase contrast (positive phase shift) was observed at the center of the particle while a dark phase contrast (negative phase shift) was observed at its periphery. By contrast, such phase shifts were not observed for particle *A*. Scale bars are 300 nm

membranes isolated from 23 prestin-transfected CHO cells and found 109 Qdots on such membranes. Since, in some cases, a few ring-like structures were found around one Qdot, 120 such structures were found in total. This histogram exhibited two main Gaussian distributions shown by red and blue lines (red, y_0=0.9±1.0, A=6.2±2.1, x_{width}= 0.5±0.2; blue, y_0=1.6±0.7, A=4.6±1.2, x_{width}=1.4±0.5). The peaks of those distributions were 9.6±0.1 nm (red) and 13.0±0.2 nm (blue), respectively.

Discussion

Sample preparation

In our previous study, the cytoplasmic surfaces of the isolated plasma membranes of CHO cells were found to be covered with protruding globular structures approximately 100 nm in diameter [18]. These protruding globular structures were colocalized with the immunofluorescence of prestin, indicating that prestin was not uniformly distributed in the plasma membrane of the prestin-transfected CHO cells. As these large structures hinder efforts to obtain AFM images at high-magnification, the images were obtained in the membrane areas without such structures in that study. In the present study, to observe the membrane topology of prestin at the nanoscale level, a flatter surface of the isolated plasma membrane was required. To obtain such flat plasma membrane sheets, therefore, the sample preparation method was modified. That is, the CHO cells were cultured in the culture medium overnight, rather than 5 min incubation in the external solution just before sonication as in the previous method. Due to this, the cell shape became flatter and more spindly, as shown in Fig. 1, compared with the cells grown by the previous method. As shown in the bottom panels of Fig. 2a, this procedure significantly reduced the number of the protruding globular structures 100 nm in diameter on the cytoplasmic faces of the isolated plasma membranes of the CHO cell.

The existence of prestin in the plasma membrane isolated from such spindle-shaped CHO cells after incubation with high-salt buffer and trypsin was confirmed by immunostaining (top panels, Fig. 2). Fluorescence labeling of the prestin-transfected CHO cells but not of the untransfected CHO cells was confirmed, suggesting that prestin existed in the isolated plasma membranes of the spindle-shaped CHO cells even after treatment with high-salt buffer and trypsin, and thus these isolated plasma membranes were applicable as samples for AFM observation.

As shown in Fig. 2c, the average thickness of the isolated plasma membranes of the prestin-transfected CHO cells was larger than that of the untransfected CHO cells by 0.82 nm with statistical significance, as shown by the asterisk (P<0.05, Student's t test). Mitra et al. [27] demonstrated that the thickness of the biological membranes was reduced up to 5 Å by depletion of the membrane proteins. Based on this report, it is likely that the increase in the thickness of the isolated plasma membrane of the prestin-transfected CHO cells in the present study was possibly due to the expression of prestin molecules.

As shown in the inset of Fig. 3a, the distribution of prestin in the plasma membrane of the CHO cells was not uniform; rather, a large amount of prestin was distributed in many spots and residual prestin was distributed in the area surrounding those spots. This distribution pattern of prestin is consistent with that observed in our previous study [18]. In that study, a considerable amount of prestin was formed to be aggregated in protruding globular structures 100 nm in diameter, which were rich in phospholipids, indicating the possible occurrence of assembly and/or disassembly of the vesicle. However, as mentioned above, in the present study, there were no such 100 nm protruding globular structures. Instead, as shown in the digital-zoomed image in Fig. 3b, the bulges about 7 nm in height were observed. By comparing the digital-zoomed image of Fig. 3b with that of Fig. 3a, such bulges and the bright patches of Qdot labeling were found to be colocalized (arrowheads shown in the insets of Fig. 3a and b). Also, as shown in Fig. 3c, magnification of the boxed area in Fig. 3b showed the existence of small bumps at the corresponding locations of the bulges observed in Fig. 3b, as indicated by dotted circles. Although the exact mechanism of the aggregation of prestin in the plasma membrane of CHO cell is still unclear, these findings support the idea that prestin may be aggregated at focal adhesion sites at an early stage or even a late stage of cell adhesion. Thus, it is likely that prestin remains at the same location, possibly in an integrin-dependent manner. However, morphological and histological studies of prestin, other proteins related to the formation of focal adhesion and the plasma membrane of the CHO cells over time using AFM, electron microscopy, confocal laser scanning microscopy, and so on are needed to obtain more detailed information concerning this mechanism.

Prestin labeling with Qdot

To label prestin molecules in the plasma membranes of a prestin-transfected CHO cells with Qdots, in the present study, the plasma membranes were isolated and incubated with antiprestin antibody and Qdot-conjugated secondary antibody. Figure 4 shows high-magnification images of such membrane. Particles 8 nm in height, corresponding to Qdots, were clearly observed. Even after scanning the sample from the top to the bottom and subsequent scanning from the bottom to the top, the location of these particles

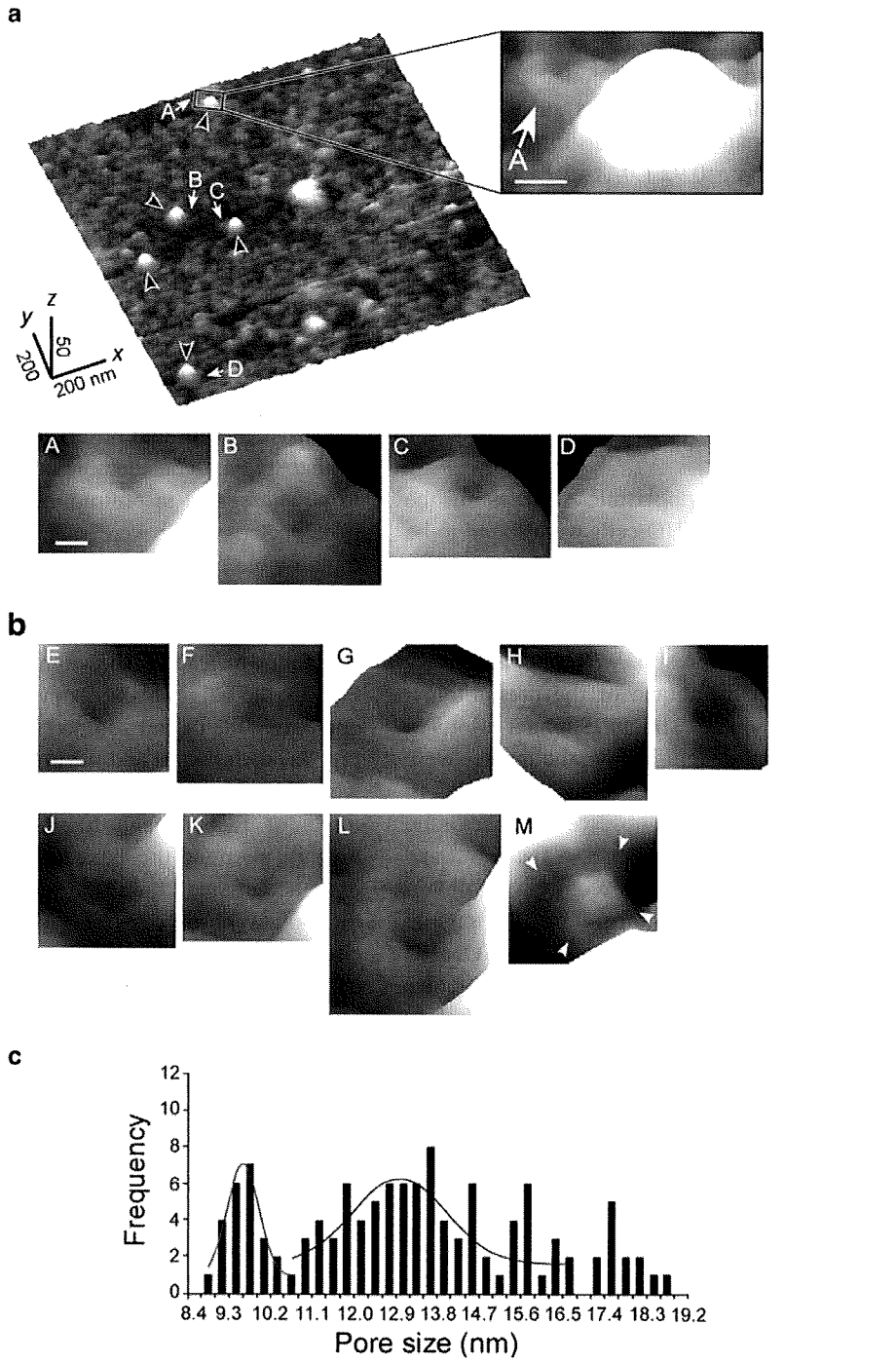

were unchanged, indicating that they were firmly attached to the isolated plasma membrane of the CHO cell. As a negative control, the plasma membrane was isolated from an untransfected CHO cell and subjected to the same sample preparation procedure. As shown in Fig. 5c, although there were a few accumulations more than 15 nm in height, probably the cytoskeletal materials and/or the peripheral proteins remained even after incubation with high-salt buffer and trypsin, no other obvious structures were seen, indicating that the Qdots did not exit.

To confirm whether the 8-nm particles observed on the isolated plasma membrane of the prestin-transfected CHO cell were Qdots, first, the size and shape of the Qdots used in the present study were measured on a mica substrate. Then, the size and shape of Qdots observed on the isolated plasma membranes were analyzed and compared with those

◀ **Fig. 8** Membrane topology of prestin on the cytoplasmic face of the plasma membrane of the prestin-transfected CHO cells. **a** High-magnification 3-D AFM images of the plasma membrane of the prestin-transfected CHO cell. Qdots 8 nm in height were clearly observed, as indicated by *black arrowheads*. As shown in the magnification at the *right*, a ring-like structure with four peaks and one valley at its center, possibly corresponding to a prestin molecule, was observed in the vicinity of the Qdot (*A*, *arrow*). Similar structures were observed at the location indicated by *arrows* (*A–D*), the magnifications of which are shown in the *bottom panels*. **b** Examples of 3-D images of the structures observed in the vicinity of the Qdots on the cytoplasmic faces of the isolated plasma membranes of the prestin-transfected CHO cells. These images were obtained from the different cells shown in **a**. Most of the observed structures are ring-like structures, each with a depression surrounded by four peaks (*E–K*). Such structures are sometimes adjacent to others, forming a unit with two molecules (*L*). Besides those ring-like structures, a square-shaped structure with a protrusion at its center, four corners of which are indicated by *arrowheads*, was also observed (*M*). The side length of the square, i.e., the length between the adjacent corners indicated by *arrowheads*, was 7.7 nm. The diameter of the protrusion was 6.2 nm. **c** Frequency distribution of the diameter of the ring-like structures (n=120) found around the Qdots (n=109) on the isolated plasma membranes of the prestin-transfected CHO cells (n=23). This histogram exhibited two main Gaussian distributions shown by *red* and *blue lines* (red, y_0=0.9±1.0, A=6.2±2.1, x_{width}=0.5±0.2; blue, y_0=1.6±0.7, A=4.6±1.2, x_{width}=1.4±0.5). The peaks of those distributions were 9.6±0.1 nm (*red*) and 13.0±0.2 nm (*blue*), respectively. Scale bars of the magnifications at the *right* and the *bottom* of **a** are 20 and 10 nm, respectively, and that of **b** is 10 nm

measured on mica. As shown in Fig. 6a, the Qdots were uniform-sized particle-like structures with a diameter of approximately 8 nm, which is in good agreement with a previously reported size of Qdots [28]. The sizes of the Qdots spread on mica showed a Gaussian distribution (red line, Fig. 6b), as did those on the isolated plasma membranes (blue line, Fig. 6b), although the distribution of the latter was much broader than that of the former. This difference may have been caused by the phospholipid membrane being relatively softer than the mica surface and/or by some materials attached to the surfaces of the Qdots and the plasma membrane, such as cell fragments and proteins contained in the culture medium, during the sample preparation. However, the average sizes of Qdots observed on the mica and the plasma membrane, i.e., 8.2±0.5 and 7.9±1.3 nm, respectively, were statistically identical (P>0.05, Student's t test; Fig. 6c), indicating that the particles 8 nm in height observed on the isolated plasma membrane of the prestin-transfected CHO cells were Qdots.

Although Qdots can be identified by checking their spherical shape and uniform size, in the present study, the existence of Qdots on the isolated plasma membrane of the CHO cell was further confirmed by using the phase imaging mode of AFM. The soft sample surface and/or the attractive interactions imposed on a tip of the AFM cantilever cause a negative phase shift, reflected as a dark phase contrast, whereas the stiff sample surface and/or the repulsive interaction between the tip and the sample cause a positive phase shift, reflected as a bright phase contrast [29]. Since the Qdots used in the present study were stiff semiconductor nanocrystals covered with soft antigoat IgG antibodies, the observed negative phase shift occurred at the peripheral part of the Qdot and the positive phase shift took place above the Qdot. Although several sizes of particles on the plasma membrane were observed in the height mode (A and B, Fig. 7a), only particle B, approximately 8 nm in height, showed a phase shift, that is, the bright phase contrast (positive phase shift) was observed at the center of the particle, whereas the dark phase contrast (negative phase shift) was observed at its periphery, suggesting that this particle was a Qdot.

Based on the two aspects mentioned above, the particles observed on the isolated plasma membranes of the prestin-transfected CHO cells were confirmed to be Qdots.

Membrane topology of prestin in the plasma membranes of CHO cells

In the present study, Qdots were used as topographic surface markers. Assuming the primary antibody binds at the tip of the N terminus and the secondary antibody conjugated with Qdot connects to the primary antibody, the maximum distance between a Qdot and a prestin molecule is estimated to be approximately 50 nm (see the "Analysis of AFM images" section). In the present study, all structures observed within 66.5 nm apart from the Qdot were subjected to the subsequent size analysis due to the architecture of the AFM system.

As shown in Fig. 8a, Qdots 8 nm in height were clearly observed on the cytoplasmic face of the isolated plasma membrane of the prestin-transfected CHO cell (black arrowheads). The magnification shown on the right revealed that a ring-like structure about 10 nm in diameter with four peaks and one valley at its center, possibly corresponding to a prestin molecule, existed in the vicinity of the Qdot. Such structures were also observed in the vicinity of Qdots indicated by the arrow (A–D, Fig. 8a), except for one Qdot, magnifications of which are shown in the bottom panels of Fig. 8a. Similarly shaped structures were also observed in the vicinity of Qdots on the cytoplasmic faces of the plasma membranes isolated from other prestin-transfected CHO cells (E–K, Fig. 8b). This configuration of prestin, i.e., four peaks at its periphery, suggests the tetrameric structure of prestin in the plasma membranes of prestin-transfected CHO cells. Sometimes, such structures are located adjacent to others (L, Fig. 8b), forming a unit with two (L, n=8), three (n=4), or four molecules (n=2). Although formation of such higher-order architectures were not frequent (approximately 14%), this